NGF-TrkA signaling in sensory nerves is required for skeletal adaptation to mechanical loads in mice

Ryan E. Tomlinson[a], Zhi Li[a], Zhu Li[a], Liliana Minichiello[b], Ryan C. Riddle[a,c], Arun Venkatesan[d], and Thomas L. Clemens[a,c,1]

[a]Department of Orthopaedic Surgery, Johns Hopkins University, Baltimore, MD 21287; [b]Department of Pharmacology, Oxford University, Oxford, OX1 3QT, United Kingdom; [c]Baltimore Veterans Administration Medical Center, Baltimore, MD 21201; and [d]Department of Neurology, Johns Hopkins University, Baltimore, MD 21287

Edited by Clifford J. Tabin, Harvard Medical School, Boston, MA, and approved March 23, 2017 (received for review January 25, 2017)

Sensory nerves emanating from the dorsal root extensively innervate the surfaces of mammalian bone, a privileged location for the regulation of biomechanical signaling. Here, we show that NGF-TrkA signaling in skeletal sensory nerves is an early response to mechanical loading of bone and is required to achieve maximal load-induced bone formation. First, the elimination of TrkA signaling in mice harboring mutant TrkA^{F592A} alleles was found to greatly attenuate load-induced bone formation induced by axial forelimb compression. Next, both in vivo mechanical loading and in vitro mechanical stretch were shown to induce the profound up-regulation of NGF in osteoblasts within 1 h of loading. Furthermore, inhibition of TrkA signaling following axial forelimb compression was observed to reduce measures of Wnt/β-catenin activity in osteocytes in the loaded bone. Finally, the administration of exogenous NGF to wild-type mice was found to significantly increase load-induced bone formation and Wnt/β-catenin activity in osteocytes. In summary, these findings demonstrate that communication between osteoblasts and sensory nerves through NGF-TrkA signaling is essential for load-induced bone formation in mice.

sensory nerves | mechanical loading | nerve growth factor | neurotrophic tyrosine kinase receptor type 1 | Wnt signaling

The skeleton of terrestrial mammals is exquisitely responsive to its mechanical environment (1, 2). Skeletal cells convert mechanical cues into biochemical signals to coordinate anabolic and catabolic processes such that new bone is formed at sites of high strain and removed in areas of low strain. This process, referred to as strain adaptive bone remodeling, enables bone mass and geometry to adapt to changing functional demands by generating bone where it is needed and eliminating bone that is underused (3).

The cellular and molecular mechanisms that mediate strain adaptive bone remodeling have been studied extensively in a variety of in vivo and in vitro experimental models. A wealth of circumstantial evidence implicates the osteocyte as the key bone cell responsible for transducing mechanical cues into downstream signaling that impacts bone turnover. Osteocytes are long-lived descendants of terminally differentiated osteoblasts that become embedded in calcified bone in great numbers (4). These cells exhibit several properties compatible with a role as a mechanosensor, including their extensive dendritic connections to bone cells throughout the skeleton (5) and their ability to produce both anabolic (Wnt/Sclerostin) and catabolic (RANKL) signaling molecules (6–8). However, the nature of the molecular signals that may act upstream of the osteocyte are less well defined.

The ability of several tissues to perceive and respond to mechanical stimuli is enabled by the somatosensory system of peripheral nerves (9). Sensory nerves emanating from the dorsal root ganglion of the spinal cord innervate tissues throughout the body and function to relay information on proprioception (spatial position) and nociception (pain) to higher centers (10). The vast majority (80%) of nerves in adult bone are thinly myelinated or unmyelinated sensory nerves that express neurotrophic tyrosine kinase receptor 1 (TrkA), the high-affinity receptor for nerve growth factor (NGF) (11, 12). Recent studies in mice have shown that TrkA sensory nerves innervate the developing femur where they facilitate formation of both primary and secondary ossification centers (13). In the mature mammalian skeleton, sensory nerves are most abundant at the periosteal and endosteal surfaces, a privileged location in bone for the regulation of biomechanical signaling.

In this study, we investigated the role of sensory nerve signaling in load-induced bone formation by using mice engineered to express mutant TrkA receptors that can be acutely disabled. Our results suggest a model in which mechanical load up-regulates NGF expression in osteoblasts, activating TrkA sensory nerves and leading to the release of osteogenic cues that modulate osteocytic Wnt signaling and support bone formation.

Results

Inhibition of TrkA Signaling Impairs Load-Induced Bone Formation. To determine the role of TrkA signaling in load-induced bone formation, we used TrkA^{F592A} mice, a chemical-genetic mouse model that allows for small molecule-mediated inhibition of TrkA signaling (14). To validate this experimental approach in adult mice, we analyzed the effectiveness of 1NMPP1 to block NGF-induced thermal and mechanical hyperalgesia, which is entirely mediated by TrkA signaling (15). Administration of 1NMPP1 [17 μg/g body weight (BW)] was sufficient to completely block the effect of a simultaneous injection of NGF (5 μg/g BW) in TrkA^{F592A} mice but not TrkA^{wt} mice (Fig. 1 *A* and *B*). In addition, TrkA^{F592A} mice had no significant differences in BW (Fig. 1*C*), femur length (Fig. 1*D*), femur strength (Fig. 1*E*), or open field behavior (Fig. 1 *F*–*I*). Thus, 1NMPP1 effectively blocks NGF signaling through its high-affinity receptor TrkA in phenotypically normal adult TrkA^{F592A} mice.

Significance

Peripheral sensory nerves expressing TrkA, the high-affinity receptor for NGF, densely innervate the surfaces of long bones, a privileged location for the regulation of biomechanical signaling. In this study, we used several genetically engineered mouse models to examine the role of NGF-TrkA signaling in skeletal adaptation to mechanical loads. Our results support a model in which mechanical signals up-regulate the expression of NGF in osteoblasts on the bone surface that, in turn, activates TrkA sensory nerves, leading to the release of osteogenic cues that modulate osteocytic Wnt/β-catenin signaling and support bone formation.

Author contributions: R.E.T. and T.L.C. designed research; R.E.T., Zhi Li, and Zhu Li performed research; L.M., R.C.R., and A.V. contributed new reagents/analytic tools; R.E.T. and T.L.C. analyzed data; and R.E.T. and T.L.C. wrote the paper.

The authors declare no conflict of interest.

This article is a PNAS Direct Submission.

[1]To whom correspondence should be addressed. Email: tclemen5@jhmi.edu.

This article contains supporting information online at www.pnas.org/lookup/suppl/doi:10.1073/pnas.1701054114/-/DCSupplemental.

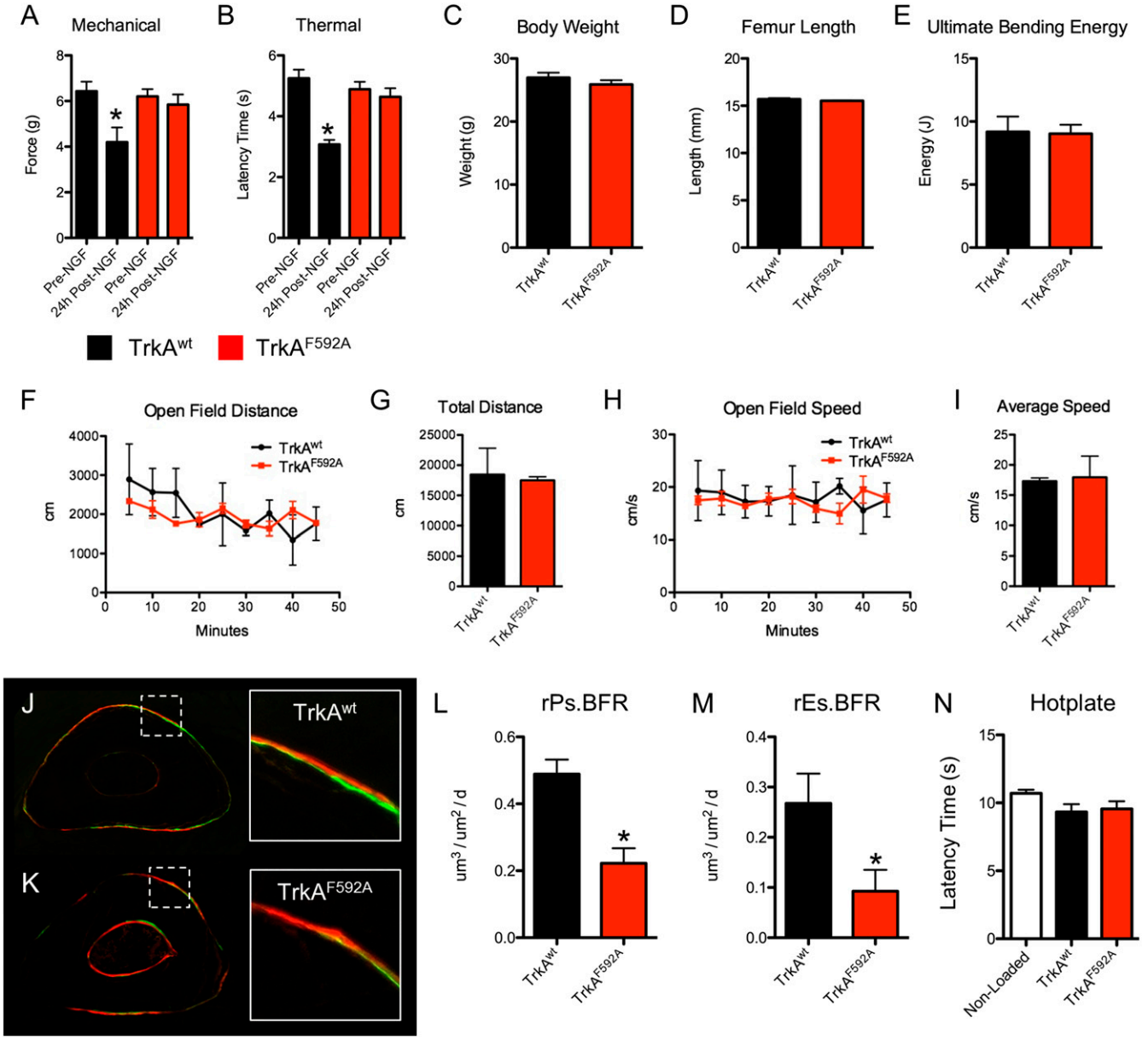

Fig. 1. Inhibition of TrkA signaling by 1NMPP1 decreases load-induced bone formation in phenotypically normal TrkA^{F592A} mice. (*A* and *B*) TrkA^{wt} and TrkA^{F592A} mice (n = 4–5) were simultaneously injected with NGF (5 μg/g BW) and 1NMPP1 (17 μg/g BW). Mechanical (*A*) and thermal (*B*) sensitivity was quantified immediately before and 24 h after treatment. (*C*–*E*) Phenotypic analysis of TrkA^{wt} and TrkA^{F592A} mice (n = 6) at 16 wk of age included body weight (*H*), femur length (*I*), or ultimate bending energy (*J*) as measured by three point bending of the femur. (*F*–*I*) Quantification of open field testing of TrkA^{wt} and TrkA^{F592A} mice (n = 3) by open field distance (*F*), total distance (*G*), open field speed (*H*), and average speed (*I*). (*J*–*N*) TrkA^{wt} and TrkA^{F592A} mice (n = 6) were subjected to 3 d of axial compression of the forelimb, with calcein and alizarin red injected 3 and 8 d after loading, respectively. Undecalcified sections from TrkA^{wt} (*J*) and TrkA^{F592A} (*K*) mice were used to quantify relative periosteal (*L*) and endosteal (*M*) bone formation rates. (*N*) Hotplate sensitivity testing was performed 3 d after loading. *P < 0.05 by t test. Data are presented as mean ± SE.

Therefore, TrkA^{F592A} mice and TrkA^{wt} littermates were subjected to three consecutive bouts of daily forelimb axial compression designed to produce lamellar bone formation. To inhibit TrkA signaling during loading, 1NMPP1 (17 μg/g BW) was administered to TrkA^{F592A} mice and TrkA^{wt} littermates 1 h before loading and provided in drinking water (40 μM) throughout the experiment. Calcein and alizarin were administered 3 and 8 d after the first bout of loading, and bone formation was assessed by dynamic histomorphometry. Axial compression produced the expected anabolic response in both genotypes of mice, with robust increases in bone formation evident on the periosteal and endosteal surfaces of loaded ulnae (Fig. 1 *J* and *K*). However, inhibition of TrkA signaling in TrkA^{F592A} mice greatly diminished the anabolic response, with relative periosteal and endosteal bone formation rates reduced by 65% and 79%, respectively (Fig. 1 *L* and *M*). These effects were primarily due to reductions in the bone formation activity of osteoblasts; the increase in mineralizing surface was not different between TrkA^{F592A} mice and TrkA^{wt} mice, but the increase in mineral apposition rate was reduced in TrkA^{F592A} mice (Table 1). Thermal sensitivity testing performed 3 d after the first bout of loading showed no significant differences between the groups (Fig. 1*N*). In total, these data strongly suggest that TrkA signaling in sensory nerves is required for a full anabolic response to exogenous mechanical loads.

Table 1. Inhibition of TrkA signaling impairs load-induced bone formation

Group	Ps.MS/BS, %	Es.MS/BS, %	Ps.MAR, μm/d	Es.MAR, μm/d	Ps.BFR/BS, $\mu m^3/\mu m^2/d$	Es.BFR/BS, $\mu m^3/\mu m^2/d$
$TrkA^{wt}$						
Loaded	0.61 ± 0.08*	0.57 ± 0.14*	1.45 ± 0.23*	1.11 ± 0.26	0.88 ± 0.13*	0.63 ± 0.17*
Nonloaded	0.37 ± 0.06	0.43 ± 0.08	0.94 ± 0.24	0.90 ± 0.20	0.35 ± 0.10	0.39 ± 0.11
$TrkA^{F592A}$						
Loaded	0.51 ± 0.11*†	0.50 ± 0.12	1.00 ± 0.13 +	0.98 ± 0.17	0.52 ± 0.14*†	0.50 ± 0.13
Nonloaded	0.33 ± 0.06	0.49 ± 0.10	0.87 ± 0.26	0.90 ± 0.17	0.28 ± 0.08	0.45 ± 0.14

Periosteal (Ps) and endosteal (Es) parameters of mineralizing surface per bone surface (MS/BS), mineral apposition rate (MAR), and bone formation rate per bone surface (BFR/BS) are presented as mean ± SD. *$P < 0.05$ vs. nonloaded. †$P < 0.05$ vs. $TrkA^{wt}$.

NGF Is Produced by Osteoblasts in Response to Mechanical Load. The finding that inhibition of TrkA signaling reduced load-induced bone formation implies that mechanical signals may regulate the production of NGF, the high-affinity ligand for the TrkA receptor (16). Therefore, we analyzed NGF expression in bone following axial forelimb compression by using mice engineered to express EGFP under the control of the full-length mouse *Ngf* promoter (NGF-EGFP mice). We found increased NGF expression in osteocalcin-expressing cells on both the endosteal and periosteal surfaces of ulna harvested from NGF-EGFP mice at 1 and 3 h after loading (Fig. 2 *A* and *B*). After 24 h, NGF expression in osteocalcin-expressing cells was still observed on endosteal, but not periosteal, surfaces (Fig. 2*C*). Relatively few NGF-expressing osteoblasts were observed in the nonloaded limbs (Fig. 2*D*), and no reporter fluorescence was observed in osteocytes at any time point. A similar pattern of expression was observed in sections from loaded limbs by using standard immunohistochemistry against NGF (Fig. S1). Consistent with this finding, quantification of mRNA extracted from the middle third of loaded and nonloaded ulnae showed significant up-regulation of NGF at 3 and 24 h after loading (Fig. 2*E*). To further establish that osteoblasts are a source of NGF in response to mechanical load, we isolated primary calvarial osteoblasts from NGF-EGFP mice and applied 180 cycles of rest-inserted 5% biaxial tension by using a Flexcell system. Consistent with the above in vivo experiments, NGF expression in these cells was significantly increased in response to stretch, as indexed by fluorescence (Fig. 2 *F–H*) and mRNA (Fig. 2*I*).

Inhibition of TrkA Signaling Impairs Load-Induced Nerve Sprouting. The local expression of NGF is known to induce nerve sprouting in a variety of contexts (17–21). Because we observed robust expression of NGF at the bone surface in response to mechanical load, we examined the peripheral nerves resident on the periosteal surface of loaded and nonloaded ulnae. Peripheral nerves were visualized by using $TrkA^{F592A}$ mice that also carried a Thy1-YFP transgene ($TrkA^{F592A}$;Thy1-YFP) that is robustly expressed in all peripheral nerves (22). Histological sections from limbs of $TrkA^{wt}$;Thy1-YFP mice harvested after three consecutive bouts of daily forelimb axial compression revealed the presence of YFP-positive nerves on the medial surface of the ulna, near the position of peak strain (Fig. 3 *A–C*). Interestingly, confocal imaging of whole-mount specimens showed clear evidence for nerve sprouting, which increased progressively from 3 to 7 d after the first bout of loading in $TrkA^{wt}$;Thy1-YFP mice but not in $TrkA^{F592A}$;Thy1-YFP mice that received 1NMPP1 (40 μM) in drinking water throughout the experiment (Fig. 3 *D–H*). In total, these data indicate that osteoblasts communicate with sensory nerves innervating the skeleton by producing NGF in response to mechanical load.

Inhibition of TrkA Signaling Impairs Load-Induced Wnt Signaling. To examine potential mechanism(s) by which TrkA signaling in sensory nerves might in turn impinge on skeletal adaptation, we examined the Wnt/β-catenin pathway. This diverse signaling network has important roles in the development and maintenance of the peripheral nervous system and is also required for a full osteogenic response to mechanical loading in bone (23, 24). To visualize Wnt/β-Catenin activation following mechanical loading, we used $TrkA^{F592A}$ mice that carried the BATGAL reporter transgene. 1NMPP1 (17 μg/g BW) was administered 1 h before loading, and $BATGAL^+$ osteocytes were quantified in loaded and nonloaded ulnae 24 h after the single bout of loading. As expected, loading significantly increased the number of $BATGAL^+$ osteocytes in loaded limbs from $TrkA^{F592A}$ and $TrkA^{wt}$ mice, as illustrated in X-Gal–stained sections (Fig. 4 *A–H*) with dorsal horn as control (Fig. S2). However, the inhibition of TrkA signaling was associated with significantly decreased percentage of osteocyte activation (Fig. 4*I*). Furthermore, quantification of mRNA extracted from the middle third of loaded and nonloaded ulnae showed the significant down-regulation of sclerostin and up-regulation of Axin2 and Naked2 in $TrkA^{wt}$ mice; these effects were significantly diminished in $TrkA^{F592A}$ mice (Fig. 4 *J–L*). To further explore the relationship between NGF-TrkA and Wnt/β-catenin signaling in the context of mechanical loading, we isolated primary calvarial osteoblasts from mice carrying floxed alleles for β-catenin, then applied 180 cycles of rest-inserted 5% biaxial tension using a Flexcell system. Cre-mediated deletion of β-catenin was confirmed by significantly diminished mRNA expression (Fig. 4*M*). As expected, the deletion of β-catenin affected load-induced Wnt signaling, as illustrated by significantly decreased Axin2 expression (Fig. 4*N*). In contrast, NGF expression was significantly increased in response to mechanical stretch and was not affected by deletion of β-catenin (Fig. 4*M*). These data suggest that load-induced expression of NGF in osteoblasts is distinct from load-induced β-catenin activation.

Exogenous NGF Enhances Load-Induced Bone Formation. Given the above observations, we hypothesized that the administration of exogenous NGF may enhance the anabolic response of bone to mechanical forces. To test this hypothesis, we administered NGF (5 μg/g BW) or vehicle 1 h before the first of three consecutive bouts of daily forelimb axial compression in wild-type mice. As before, calcein and alizarin were administered 3 and 8 d after the first bout of loading, mice were killed at day 10, and loaded and nonloaded forelimbs were processed for dynamic histomorphometry (Fig. 5 *A* and *B*). In this scenario, administration of NGF profoundly increased the anabolic response of bone, with relative periosteal and endosteal bone formation rates increased by 128% and 142%, respectively (Fig. 5 *C* and *D*). Consistent with data from $TrkA^{F592A}$ mice, the effect of NGF was primarily to increase osteoblast activity, as evidenced by large increases in mineral apposition rate and minimal alterations in mineralizing surface (Table 2). As a control for NGF efficacy throughout the loading period, we performed thermal sensitivity testing 24 h after the third and final loading bout. As expected, mice that received NGF had developed significant thermal hyperalgesia lasting for the entire loading period (Fig. 5*E*). In a separate experiment, BATGAL mice were subjected to loading 1 h after administration of NGF (5 μg/g BW) or vehicle, and bones were harvested for X-Gal staining after 24 h (Fig. 5 *F–I*). Administration of NGF was associated with an increased percentage

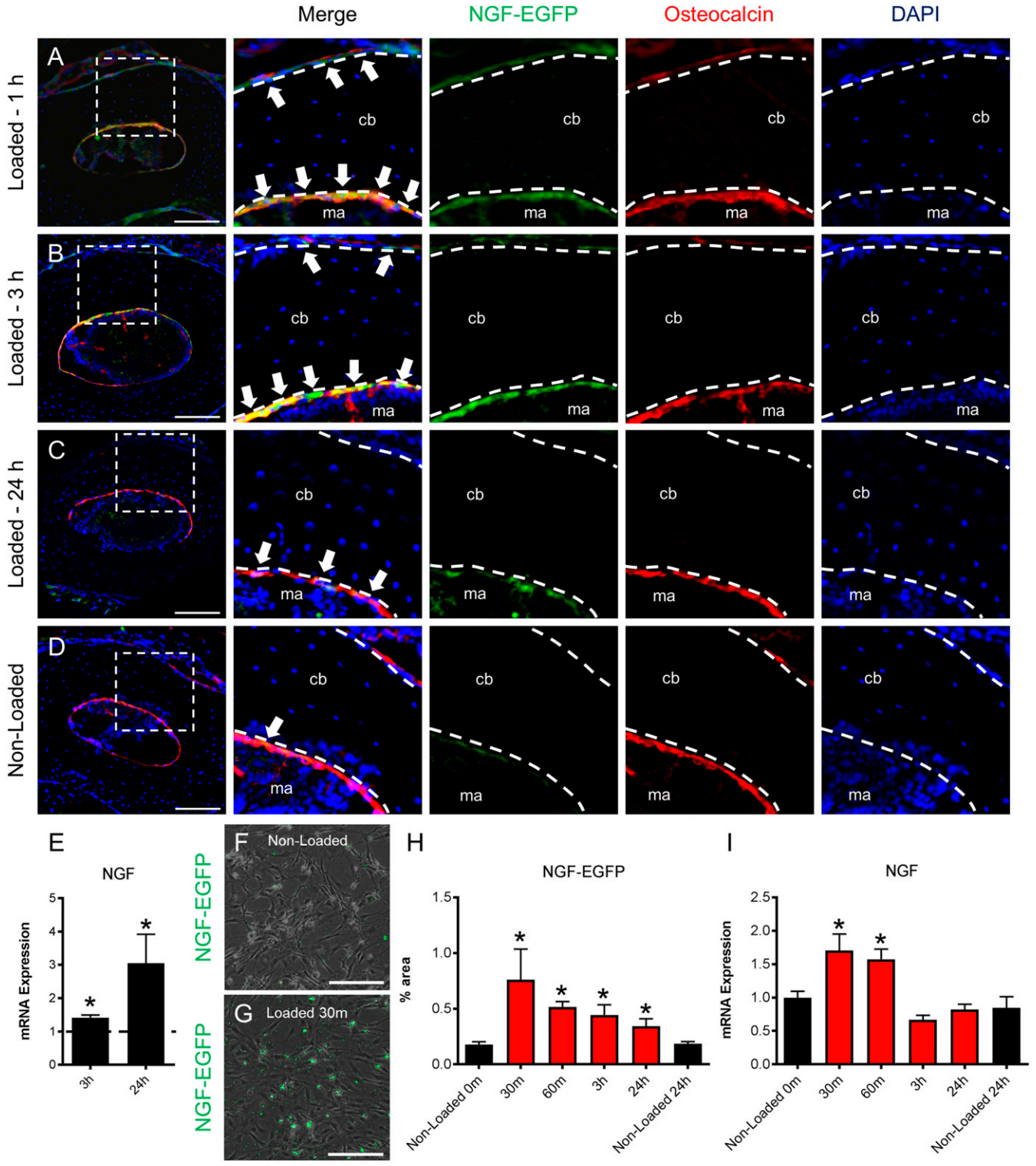

Fig. 2. NGF is expressed by osteocalcin-expressing osteoblasts following mechanical loading. (*A–D*) Forelimbs from NGF-EGFP mice were harvested for immunohistochemistry against osteocalcin at 1 h (*A*) 3 h (*B*), and 24 h (*C*) after loading, with nonloaded limbs used as controls ($n = 3$ per time point) (*D*). Arrows indicate colocalization. (*E*) mRNA expression of NGF by quantitative RT-PCR (qRT-PCR) in loaded limbs normalized to nonloaded limbs at 3 and 24 h after loading ($n = 4$). (*F–I*) Primary calvarial osteoblasts were harvested from NGF-EGFP mice and subjected to biaxial stretch. Representative fluorescence images merged with brightfield illustrate NGF expression in osteoblasts before loading (*F*) and osteoblasts 30 min after loading (*G*), with quantification at all time points ($n = 3$) (*H*). (*I*) mRNA expression of NGF by qRT-PCR in osteoblasts after mechanical stretch ($n = 3$). *$P < 0.05$ by *t* test. Data are presented as mean ± SE.

of X-Gal–positive osteocytes compared with vehicle (Fig. 5*J*). In total, these data indicate that exogenous NGF enhances load-induced bone formation by antagonizing TrkA sensory nerves in bone, although we cannot rule out the possibility that exogenous NGF might exert some activity through its low-affinity receptor p75.

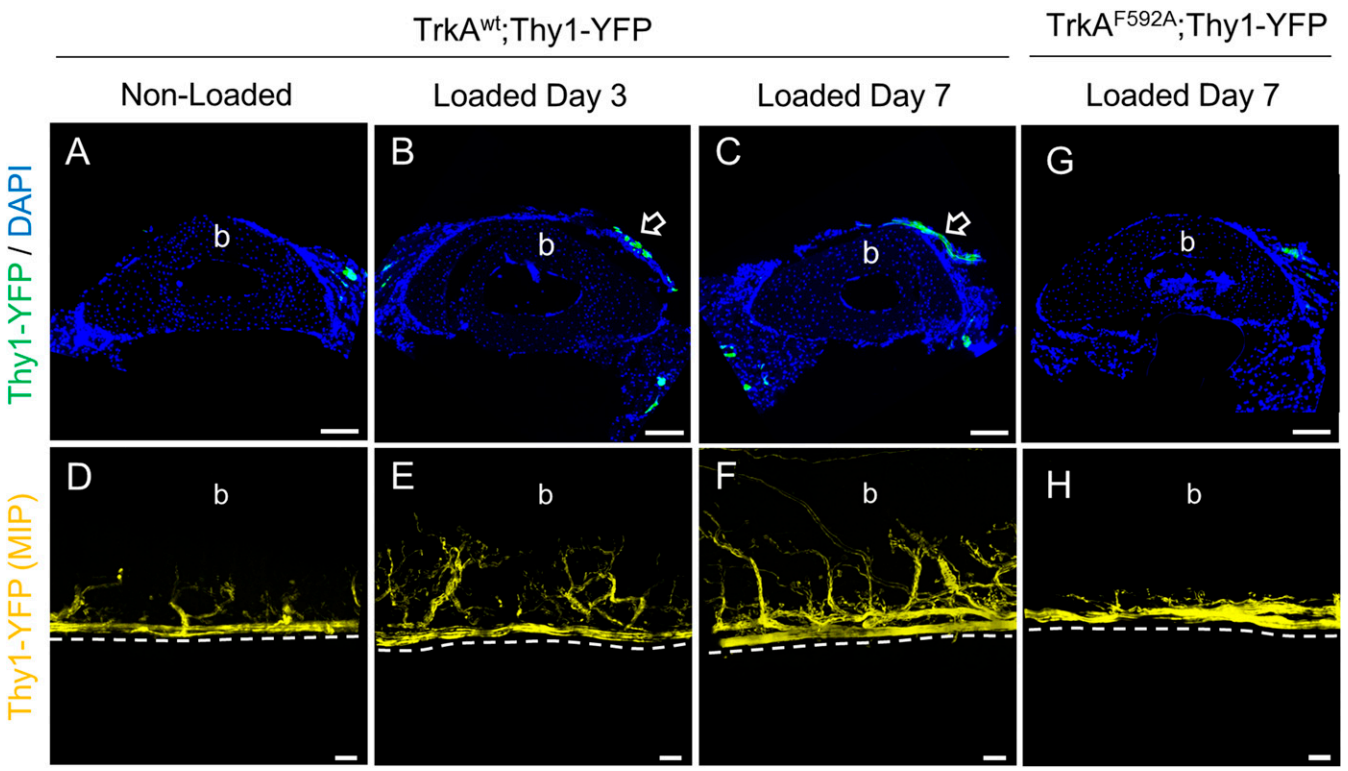

Fig. 3. Inhibition of TrkA signaling impairs load-induced nerve sprouting on the ulnar periosteal surface. (A-C) Nerves were visualized at the ulnar mid-diaphysis in Thy1-YFP mice that did not receive 1NMPP1, with representative cross-sections from nonloaded (*A*), Day 3 (*B*), and Day 7 (*C*) loaded limbs. Arrows indicate nerves visible on the medial surface. The cortical bone of the ulna is indicated as b. (*D–F*) Nerves were also visualized on the periosteal surface of the intact ulna in Thy1-YFP mice that did not receive 1NMPP1 by using confocal microscopy, with representative maximum intensity projections (MIP) from nonloaded (*D*), Day 3 (*E*), and Day 7 (*F*) loaded limbs. The periosteal surface of the ulna is indicated as b. (*G* and *H*) Nerves were visualized in TrkA^{F592A} mice that received 1NMPP1 (40 μM) to inhibit TrkA signaling following load, with representative images from cross-sections (*G*) and MIP (*H*) 7 d after loading.

Discussion

Recent studies from our laboratory in mice have shown that NGF-TrkA signaling in sensory nerves during late embryogenesis is required for normal vascularization and ossification of endochondral bone (13). The present study provides direct evidence that TrkA sensory nerves also function in postnatal bone to potentiate the anabolic response to mechanical stimuli (Fig. 6). The striking reduction in load-induced bone formation following inhibition of TrkA signaling in vivo and the amplification of load-induced bone formation in mice treated with exogenous NGF provides strong support for this conclusion.

The axial forelimb compression approach used in our studies was designed to focus on the early events of strain adaptive bone remodeling at the surface of long bones where the density of TrkA sensory nerves is highest (11, 12). The acute up-regulation of NGF in osteoblasts on both the periosteal and endosteal ulnar surfaces strongly suggests that sensory nerves located at these sites respond to this stimulus through NGF-TrkA signaling. Importantly, osteocytes did not express NGF but showed robust β-catenin reporter activity following loading, consistent with previous studies (25). Moreover, our in vitro studies showed that deletion of β-catenin in osteoblasts did not affect load-induced expression of NGF. These results suggest that osteoblasts and osteocytes respond to in vivo skeletal loads through distinct, although possibly overlapping, mechanisms. In this regard, previous studies that measured the absolute magnitude and type of force that impact bone cells during mechanical loading have shown that osteocytes experience in vivo strains that are distinct from the surface strains sensed by osteoblasts (25–29).

The cellular and molecular events through which sensory nerve signals activate osteoanabolic pathways in response to loading appear to differ in several ways from those that account for bone formation during development. Our previous studies showed that NGF is expressed in early osteochondral progenitors and is critical for the survival of TrkA sensory nerves that coordinate the vascularization and ossification of developing bone (13). However, in adult bone, NGF is no longer required for the survival of TrkA sensory nerves; rather, its expression in bone is primarily associated with osseous pain (30). Here, we show that NGF is induced by physiological mechanical forces in osteoblasts where it can activate NGF signaling in resident nerve axons. This mechanism is a consequence of the neurotrophic signaling that occurs during the formation of primary and secondary ossification centers, ensuring the survival of sensory nerves that will express TrkA (and remain sensitive to NGF) in adulthood (31). In addition, the loss of NGF-TrkA signaling during embryogenesis strongly diminished skeletal vascularization, potentially due to the role of sensory nerves as a template for developing blood vessels (32). However, vascular influences in the process of load-induced bone formation appear to be limited; the complete abrogration of angiogenesis in rats did not reduce load-induced bone formation (33), and other studies have ruled out any effect of the modulation of sympathetic tone on this process (34).

Precisely how NGF-TrkA signaling in sensory nerves influences bone homeostasis following mechanical loading remains to be determined. In other cell types, increased NGF expression in response to mechanical signals is associated with nerve sprouting and enhanced pain sensation (17–21). Although we observed load-induced nerve sprouting at the ulnar surface, loading alone was not associated with lasting pain or hyperalgesia. Our finding that load-induced Wnt/β-catenin signaling in osteocytes was regulated by NGF-TrkA signaling suggests that the activation of

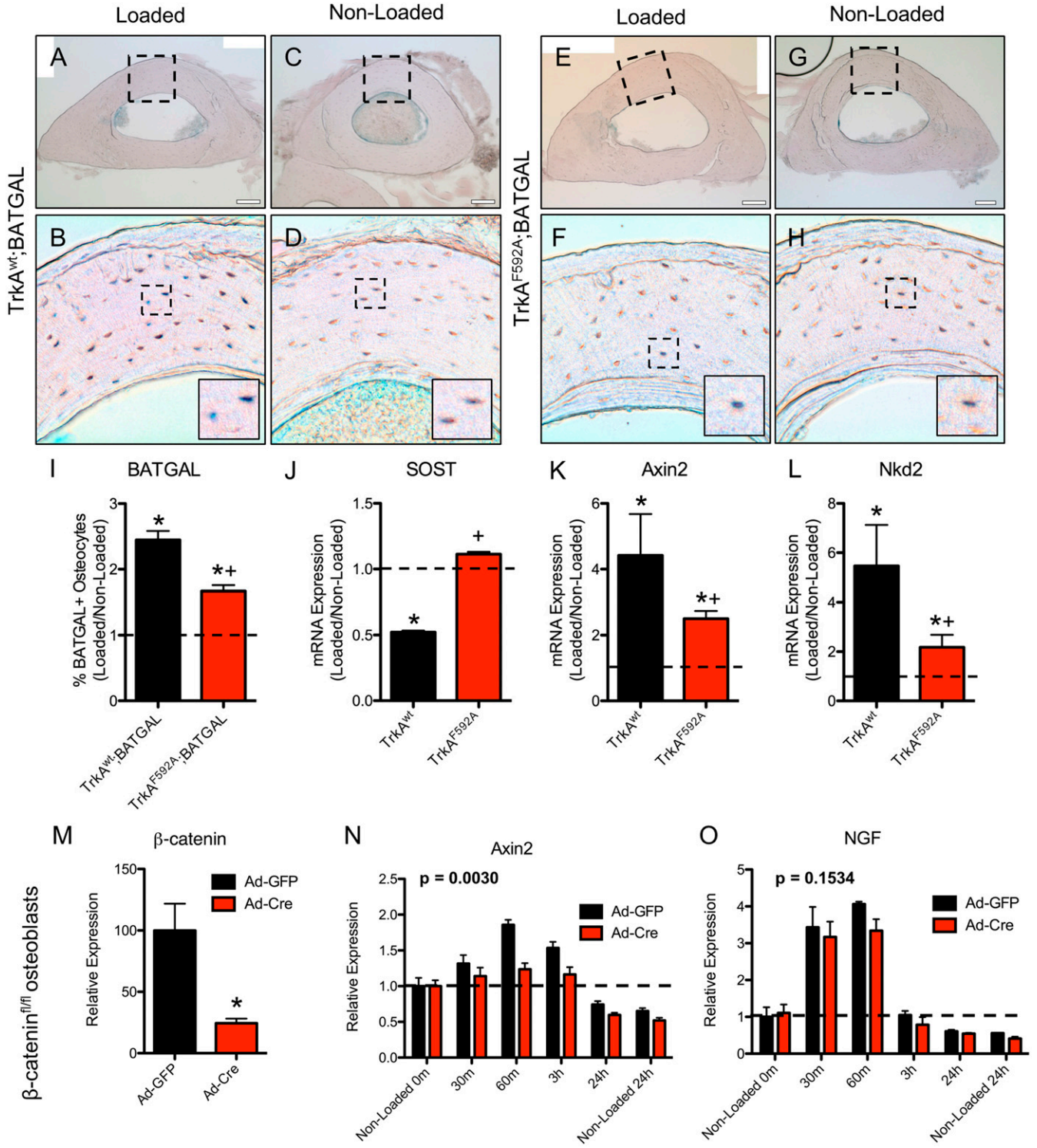

Fig. 4. Inhibition of TrkA signaling impaired load-induced osteocytic Wnt signaling. (*A–I*) Sections of loaded and nonloaded limbs from TrkA^{wt} (*A–D*) and TrkA^{F592A} (*E–H*) mice harboring the BATGAL transgene were X-Gal stained 24 h after a single bout of loading and quantified (*I*). (*J–L*) mRNA expression of Wnt signaling targets by qRT-PCR in samples taken from the middiaphysis of the ulna 24 h after loading, including SOST (*J*), Axin2 (*K*), and Naked2 (*L*). (*M–O*) Primary calvarial osteoblasts were harvested from β-catenin–floxed mice for biaxial stretching. (*M*) mRNA expression of β-catenin by qRT-PCR in osteoblasts treated with Ad-GFP or Ad-Cre. Following mechanical stretch, mRNA expression of Axin2 (*N*) and NGF (*O*) by qRT-PCR in osteoblasts treated with Ad-GFP or Ad-Cre. *$P <$ 0.05 vs. nonloaded by *t* test, + $P < 0.05$ vs. TrkA^{wt} by *t* test. *P* values noted in *N* and *O* reference the effect of treatment by two-way ANOVA.

canonical Wnt signaling is the downstream osteoanabolic mechanism. However, because osteoblasts do not express TrkA or respond to TrkA inhibition (13), it is unlikely that NGF stimulates Wnt/β-catenin signaling in osteocytes directly. In this regard, Wnt ligands are known to be sequestered in nerve axons (35) and NGF-TrkA signaling in sensory nerves promotes the

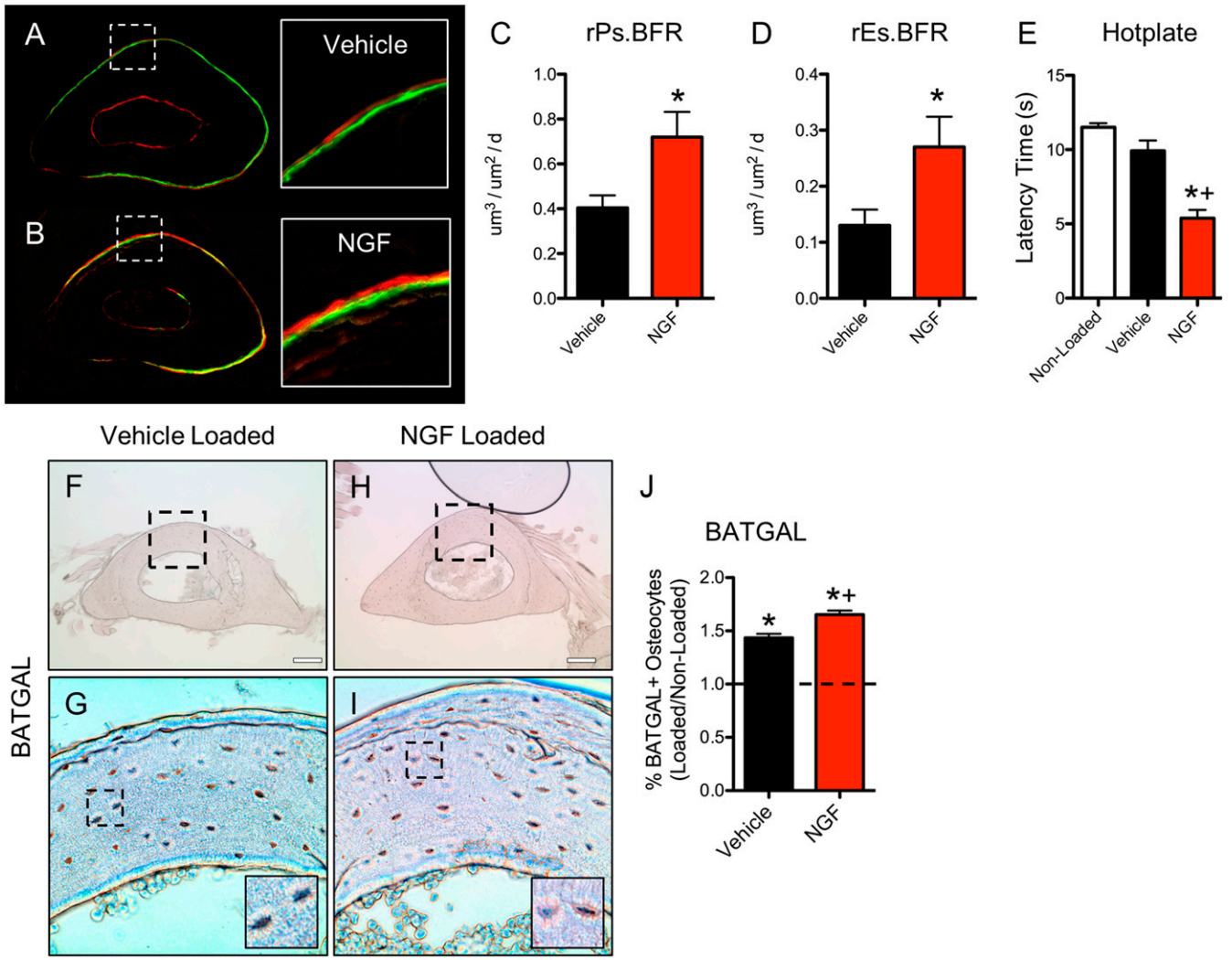

Fig. 5. Exogenous NGF increases load-induced bone formation by stimulating osteocytic Wnt signaling. (*A–E*) Wild-type mice ($n = 6$) were subjected to 3 d of axial compression of the forelimb, with calcein and alizarin red injected 3 and 8 d after loading, respectively. Undecalcified sections from mice injected with Vehicle (*A*) or NGF (5 μg/g BW) (*B*) were used to quantify relative periosteal (*C*) and endosteal (*D*) bone formation rates. (*E*) Hotplate sensitivity testing was performed 3 d after loading. (*F–J*) Sections of loaded limbs from Vehicle (*F* and *G*) and NGF (5 μg/g BW) (*H* and *I*) treated mice harboring the BATGAL transgene were X-Gal stained 24 h after a single bout of loading and quantified (*I*). *$P < 0.05$ vs. nonloaded, +$P < 0.05$ vs. Vehicle. Data are presented as mean ± SE.

localization of β-catenin at the axon tip by activating PI3K to inhibit GSK3β (36). Alternatively, NGF-TrkA signaling in sensory nerve axons is known to regulate the activity of a variety of ion channels, receptors, and secreted molecules (37), including calcitonin gene-related peptide (CGRP) and Substance P (SP) (38, 39); both CGRP and SP positively influence bone formation (40–44), and recent work has shown that mice lacking CGRP have diminished adaptation to mechanical loading (45). Such findings are consistent with other data showing that destruction of capsaicin-sensitive small neurons resulted in diminished bone volume and density, particularly in the trabecular bone compartment (46, 47). However, more study is required to determine whether these or other signals are downstream of NGF-TrkA signaling in strain-adaptive bone remodeling.

The recognition that sensory nerves have an important role in regulating the anabolic response of bone to mechanical loading has direct relevance to human bone. First, these data may help to explain anecdotal clinical evidence of skeletal disorders in patients with congenital insensitivity to pain with anhidrosis (CIPA), caused by loss-of-function mutations in either NGF or TrkA (48–51). In addition, our studies suggest the feasibility for developing strategies that positively modulate load-induced bone formation and/or prevent bone loss due to age and disease by targeting sensory nerve signals. Finally, our results suggest that the anti-TrkA and anti-NGF antibodies being developed to combat musculoskeletal pain may negatively affect bone mass accrual over time, particularly in patients engaged in repetitive weight bearing activity (37, 52, 53).

Methods

Mice. All procedures involving mice were approved by the Institutional Animal Care and Use Committee of The Johns Hopkins University (protocol M015M118). $TrkA^{F592A}$ mice, which harbor a phenylalanine-to-alanine point mutation in exon 12 of the mouse *Ntrk1* gene (F592A) that renders the endogenous TrkA kinase sensitive to inhibition by the membrane-permeable small molecule 1NMPP1 (14), are commercially available (Jackson Laboratory; stock no. 022362). Thy1-YFP mice, which express a transgene derived from the mouse *Thy1* gene to drive expression of YFP in nerves (22), are commercially available (Jackson Laboratory; stock no. 003709). NGF-EGFP mice, which express EGFP under the control of the full-length mouse *Ngf* promoter, were generously donated by the Kawaja Laboratory (54). Mice with floxed *Ctnnb1* (β-catenin) alleles were obtained from Jackson Laboratory (stock no. 004152)

Table 2. Exogenous NGF increases load-induced bone formation

Group	Ps.MS/BS, %	Es.MS/BS, %	Ps.MAR, μm/d	Es.MAR, μm/d	Ps.BFR/BS, $\mu m^3/\mu m^2/d$	Es.BFR/BS, $\mu m^3/\mu m^2/d$
Vehicle						
Loaded	0.55 ± 0.12*	0.38 ± 0.10	1.34 ± 0.32*	1.07 ± 0.29	0.73 ± 0.20*	0.42 ± 0.09*
Nonloaded	0.30 ± 0.10	0.32 ± 0.08	1.05 ± 0.22	0.88 ± 0.30	0.33 ± 0.11	0.29 ± 0.11
NGF						
Loaded	0.63 ± 0.12*	0.45 ± 0.07*	1.63 ± 0.37*	1.37 ± 0.29*†	1.04 ± 0.39*†	0.62 ± 0.18*†
Nonloaded	0.30 ± 0.10	0.37 ± 0.08	0.97 ± 0.17	0.91 ± 0.22	0.32 ± 0.10	0.35 ± 0.12

Periosteal (Ps) and endosteal (Es) parameters of mineralizing surface per bone surface (MS/BS), mineral apposition rate (MAR), and bone formation rate per bone surface (BFR/BS) are presented as mean ± SD. *$P < 0.05$ vs. nonloaded. †$P < 0.05$ vs. vehicle.

and have been validated (55). Analyses were performed while blinded to genotype.

Mechanical Loading. Mechanical loading of female adult mice (16–20 wk) was performed daily for up to three consecutive days, as described (56, 57). Mice were anesthetized by using isoflurane gas (1–3%) for the duration of the experiment. After confirming deep anesthesia, the right forelimb was axially compressed by placing the olecranon process and the flexed carpus into specially designed fixtures. A material testing system (TA Systems Electroforce 3200 Series II) was used to apply force and monitor displacement. A 0.3 N compressive preload was applied followed by a cyclic rest-inserted trapezoidal waveform with a peak force of 3.0 N at 0.1 Hz for 100 cycles. After loading, mice were given an intramuscular injection of analgesic (0.05 mg/kg buprenorphine) and allowed unrestricted cage activity.

Dynamic Histomorphometry. Bone formation rates were quantified by dynamic histomorphometry. Mice were given two i.p. injections of fluorescent bone formation markers: calcein (10 mg/kg; Sigma C0875) was administered 3 d after loading and alizarin (30 mg/kg; Sigma A3882) was administered at day 8. Forelimbs were harvested 10 d after loading, fixed overnight in 4% PFA, and embedded in polymethylmethacrylate before sectioning at 100 μm (Leco VC50). After mounting on glass slides, sections were polished to 30 μm and imaged by using fluorescence microscopy (Olympus IX-71). Images were analyzed for endosteal (Es) and periosteal (Ps) mineralizing surface (MS/BS), mineral apposition rate (MAR), and bone formation rate (BFR/BS), as defined by the ASBMR Committee for Histomorphometry Nomenclature (58).

Synthesis and Administration of 1NMPP1. 1NMPP1 (lot no. 51–180-51) was synthesized by Aurora Analytics LLC using standard techniques (59). Purity (99.2%) was confirmed by HPLC-UV254, and characterization by ^{1}H NMR (400 MHz, DMSO-d6) was consistent with structure. Stock solution was prepared at 200 mM by dissolving 1NMPP1 powder in DMSO. i.p. injections were performed by using a 5 mM solution at a dosage of 17 μg/g BW. Drinking water was prepared at 40 μM in ddH_2O with 1% PBS-Tween 20.

Behavioral and Sensitivity Testing. Behavioral analysis was performed by the Johns Hopkins Behavioral Core. Open field testing was used to determine overall locomotor activity by placing mice into a custom-made acrylic chamber and allowing the mice to explore the chamber for 60 min, as described (60). Thermal and mechanical sensitivity testing was performed by standard Von Frey and Hargreaves testing protocols, as described (61, 62). Hotplate sensitivity testing was used to determine the response time of each mouse to a hot plate maintained at 55 °C, as described (63).

Histology. Intact forelimbs were harvested and placed in 4% PFA at 4 °C for 16–24 h. After three washes in PBS, samples were decalcified in 14% EDTA (1:20 volume) for up to 14 d at 4 °C. Next, samples were sunk in 30% sucrose overnight at 4 °C before embedding in O.C.T. media (Tissue-Tek). Sections were cut and mounted on adhesive slides (TruBond 380). For immunohistochemistry, sections were thoroughly washed, blocked by using PBS with 1.5% normal serum, and incubated in primary antibody (sc-30045 or sc-548; Santa Cruz) overnight at 4 °C in a humidified chamber. The following day, slides were washed, incubated in fluorescent secondary antibody for 1 h at 4 °C, then mounted by using media containing DAPI (Vectashield H-1200). Digital images of these sections were captured with a 10× or 20× objective (Olympus IX-71). Imaging stitching and quantification was performed by using FIJI (64).

Osteoblast Culture and Viral Transfection. Osteoblasts were isolated from calvaria of newborn mice by serial digestion in 1.8 mg/mL collagenase type I, as described (65). The cells were then grown to confluency in αMEM containing 10% FBS and 1% penicillin/streptomycin in a 37 °C humidified incubator at 5% CO_2. To abolish expression of β-catenin in vitro, osteoblasts from mice harboring floxed alleles were infected with adenovirus encoding Cre recombinase (Ad-Cre) or green fluorescent protein (Ad-GFP) obtained from Vector Biolabs. All infections were performed with an MOI of 100.

Flexcell Stretching. Primary osteoblasts were plated at 5,000 cells per cm^2 in collagen-coated Flexcell plates in αMEM containing 10% FBS. After allowing cells to attach for 24–48 h, cells were serum-starved (αMEM containing 1% FBS) overnight. For fluorescence imaging, αMEM was replaced with 1× Opti-Klear media (Marker Gene Technologies). The Flexcell FX-5000T was used to stretch cells by using a cyclic rest-inserted waveform with a peak biaxial stretch of 5% at 0.1 Hz for 180 cycles. NGF expression was assayed by using live cell fluorescence imaging (Olympus IX-71).

Gene Expression by Quantitative RT-PCR. Total RNA was collected by using TRIzol (Life Technologies) according to the manufacturer's protocol. RNA (1 μg) was then reversely transcribed by using an iScript cDNA Synthesis Kit (Bio-Rad). cDNA (2 μL) was then amplified under standard PCR conditions by using iQ

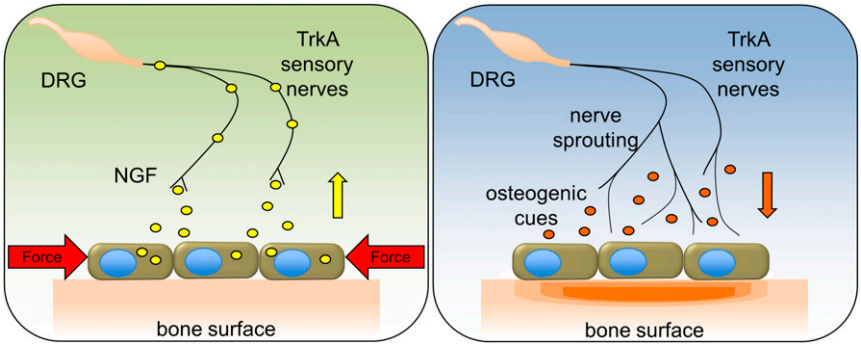

Fig. 6. Schematic of NGF-TrkA signaling in load-induced bone formation. In response to mechanical forces, osteoblasts release NGF that activates TrkA sensory nerves. Downstream NGF-TrkA signaling in nerves induces nerve sprouting on the periosteal surface and the release of osteogenic cues to stimulate bone formation.

SYBR Green Supermix (Bio-Rad). All cDNA samples were run in triplicate, averaged, and normalized to endogenous β-actin expression levels. Primer sequences were designed by using Primer-BLAST (NCBI) and are available upon request.

Clearing and Confocal Imaging. Samples were harvested under a dissecting microscope to remove muscle and soft tissue, then placed in 4% PFA at 4 °C for 16–24 h. After three washes in PBS and decalcification in 14% EDTA (1:20 volume) for up to 14 d at 4 °C, samples were optically cleared by using a modified SeeDB method (66). Briefly, samples were immersed in increasing concentrations of D-(−)-Fructose (F3510, Sigma), with 0.5% α-thioglycerol (M1753, Sigma), up to a maximum concentration of 80.2% (wt/wt) fructose with gentle shaking at room temperature. After obtaining sufficient clarity, intact samples were mounted on coverslips and imaged by using confocal microscopy (Zeiss 780 LSM).

X-Gal Staining. The staining protocol was adapted from previous work (25). Briefly, samples were carefully harvested under a dissecting microscope to remove muscle without damaging the periosteum, then placed into fresh 4% PFA (Alfa Aesar no. 43368) at 4 °C for 75 min. Next, samples were placed into fresh X-Gal staining solution, which contained 1 mL of X-Gal stock (40 mg of X-Gal in 1 mL of DMF), 1 mL of 0.2 M potassium ferricyanide, 1 mL of 0.2 M potassium ferrocyanide, 400 μL of 1 M Tris·HCl (pH 8.0), and 36.6 mL of X-Gal Buffer (1 mL of 1 M $MgCl_2$, 100 μL of Nonidet P-40, and 50 mg of sodium deoxycholate in 500 mL of ddH_2O), for 36–48 h at 32 °C without shaking. Samples were then postfixed by using 4% PFA at 4 °C. Decalcification was performed for 7 d in 14% EDTA at 4 °C with shaking. After decalcification was complete, samples were sunk in 30% sucrose and then embedded in OCT for sectioning. Finally, sections were mounted and imaged by using bright-field microscopy (Olympus IX-71). Between each step of processing, bones were thoroughly washed by using three changes of PBS for 5 min each.

Statistics. All results are presented as mean ± SE, unless otherwise noted. Statistical analyses were performed in Prism (GraphPad) by using unpaired, two-tailed Student's *t* tests or two-way ANOVA. A *P* value of less than 0.05 was considered significant.

ACKNOWLEDGMENTS. We thank Drs. David Ginty and Michael Kawaja for supplying mice used in this study and Dr. Mark Johnson for help with staining. This work was supported by National Institutes of Health Grant AR068934 (to T.L.C.). T.L.C. is the recipient of a Senior Research Career Scientist Award from the Department of Veterans Affairs.

1. Frost HM (1963) Measurement of human bone formation by means of tetracycline labelling. *Can J Biochem Physiol* 41:31–42.
2. Robling AG, Castillo AB, Turner CH (2006) Biomechanical and molecular regulation of bone remodeling. *Annu Rev Biomed Eng* 8:455–498.
3. Seeman E (2009) Bone modeling and remodeling. *Crit Rev Eukaryot Gene Expr* 19: 219–233.
4. Bonewald LF (2011) The amazing osteocyte. *J Bone Miner Res* 26:229–238.
5. Bonewald LF (2005) Generation and function of osteocyte dendritic processes. *J Musculoskelet Neuronal Interact* 5:321–324.
6. Xiong J, et al. (2015) Osteocytes, not osteoblasts or lining cells, are the main source of the RANKL required for osteoclast formation in remodeling bone. *PLoS One* 10: e0138189.
7. van Bezooijen RL, et al. (2004) Sclerostin is an osteocyte-expressed negative regulator of bone formation, but not a classical BMP antagonist. *J Exp Med* 199:805–814.
8. Klein-Nulend J, et al. (1995) Sensitivity of osteocytes to biomechanical stress in vitro. *FASEB J* 9:441–445.
9. Jones LA, Smith AM (2014) Tactile sensory system: Encoding from the periphery to the cortex. *Wiley Interdiscip Rev Syst Biol Med* 6:279–287.
10. Proske U, Gandevia SC (2012) The proprioceptive senses: Their roles in signaling body shape, body position and movement, and muscle force. *Physiol Rev* 92:1651–1697.
11. Jimenez-Andrade JM, et al. (2010) A phenotypically restricted set of primary afferent nerve fibers innervate the bone versus skin: Therapeutic opportunity for treating skeletal pain. *Bone* 46:306–313.
12. Castañeda-Corral G, et al. (2011) The majority of myelinated and unmyelinated sensory nerve fibers that innervate bone express the tropomyosin receptor kinase A. *Neuroscience* 178:196–207.
13. Tomlinson RE, et al. (2016) NGF-TrkA signaling by sensory nerves coordinates the vascularization and ossification of developing endochondral bone. *Cell Reports* 16: 2723–2735.
14. Chen X, et al. (2005) A chemical-genetic approach to studying neurotrophin signaling. *Neuron* 46:13–21.
15. Bergmann I, Reiter R, Toyka KV, Koltzenburg M (1998) Nerve growth factor evokes hyperalgesia in mice lacking the low-affinity neurotrophin receptor p75. *Neurosci Lett* 255:87–90.
16. Levi-Montalcini R, Skaper SD, Dal Toso R, Petrelli L, Leon A (1996) Nerve growth factor: From neurotrophin to neurokine. *Trends Neurosci* 19:514–520.
17. Persson K, Sando JJ, Tuttle JB, Steers WD (1995) Protein kinase C in cyclic stretch-induced nerve growth factor production by urinary tract smooth muscle cells. *Am J Physiol* 269:C1018–C1024.
18. Clemow DB, Steers WD, Tuttle JB (2000) Stretch-activated signaling of nerve growth factor secretion in bladder and vascular smooth muscle cells from hypertensive and hyperactive rats. *J Cell Physiol* 183:289–300.
19. Rana OR, et al. (2010) Mechanical stretch induces nerve sprouting in rat sympathetic neurocytes. *Auton Neurosci* 155:25–32.
20. Saygili E, et al. (2011) Mechanical stretch of sympathetic neurons induces VEGF expression via a NGF and CNTF signaling pathway. *Biochem Biophys Res Commun* 410: 62–67.
21. Pecchi E, et al. (2014) Induction of nerve growth factor expression and release by mechanical and inflammatory stimuli in chondrocytes: Possible involvement in osteoarthritis pain. *Arthritis Res Ther* 16:R16.
22. Feng G, et al. (2000) Imaging neuronal subsets in transgenic mice expressing multiple spectral variants of GFP. *Neuron* 28:41–51.
23. Hens JR, et al. (2005) TOPGAL mice show that the canonical Wnt signaling pathway is active during bone development and growth and is activated by mechanical loading in vitro. *J Bone Miner Res* 20:1103–1113.
24. Robinson JA, et al. (2006) Wnt/beta-catenin signaling is a normal physiological response to mechanical loading in bone. *J Biol Chem* 281:31720–31728.
25. Lara-Castillo N, et al. (2015) In vivo mechanical loading rapidly activates β-catenin signaling in osteocytes through a prostaglandin mediated mechanism. *Bone* 76: 58–66.
26. Bonivtch AR, Bonewald LF, Nicolella DP (2007) Tissue strain amplification at the osteocyte lacuna: A microstructural finite element analysis. *J Biomech* 40:2199–2206.
27. Bonewald LF, Johnson ML (2008) Osteocytes, mechanosensing and Wnt signaling. *Bone* 42:606–615.
28. Moustafa A, et al. (2012) Mechanical loading-related changes in osteocyte sclerostin expression in mice are more closely associated with the subsequent osteogenic response than the peak strains engendered. *Osteoporos Int* 23:1225–1234.
29. Schaffler MB, Cheung WY, Majeska R, Kennedy O (2014) Osteocytes: Master orchestrators of bone. *Calcif Tissue Int* 94:5–24.
30. Mantyh PW (2014) The neurobiology of skeletal pain. *Eur J Neurosci* 39:508–519.
31. Oppenheim RW (1989) The neurotrophic theory and naturally occurring motoneuron death. *Trends Neurosci* 12:252–255.
32. Mukouyama YS, Shin D, Britsch S, Taniguchi M, Anderson DJ (2002) Sensory nerves determine the pattern of arterial differentiation and blood vessel branching in the skin. *Cell* 109:693–705.
33. Tomlinson RE, Schmieder AH, Quirk JD, Lanza GM, Silva MJ (2014) Antagonizing the αv β3 integrin inhibits angiogenesis and impairs woven but not lamellar bone formation induced by mechanical loading. *J Bone Miner Res* 29:1970–1980.
34. de Souza RL, Pitsillides AA, Lanyon LE, Skerry TM, Chenu C (2005) Sympathetic nervous system does not mediate the load-induced cortical new bone formation. *J Bone Miner Res* 20:2159–2168.
35. Inestrosa NC, Arenas E (2010) Emerging roles of Wnts in the adult nervous system. *Nat Rev Neurosci* 11:77–86.
36. Zhou FQ, Zhou J, Dedhar S, Wu YH, Snider WD (2004) NGF-induced axon growth is mediated by localized inactivation of GSK-3β and functions of the microtubule plus end binding protein APC. *Neuron* 42:897–912.
37. Mantyh PW, Koltzenburg M, Mendell LM, Tive L, Shelton DL (2011) Antagonism of nerve growth factor-TrkA signaling and the relief of pain. *Anesthesiology* 115: 189–204.
38. Malcangio M, Garrett NE, Tomlinson DR (1997) Nerve growth factor treatment increases stimulus-evoked release of sensory neuropeptides in the rat spinal cord. *Eur J Neurosci* 9:1101–1104.
39. Quarcoo D, et al. (2004) Nerve growth factor induces increased airway inflammation via a neuropeptide-dependent mechanism in a transgenic animal model of allergic airway inflammation. *Clin Exp Allergy* 34:1146–1151.
40. Goto T, Kido MA, Yamaza T, Tanaka T (2001) Substance P and substance P receptors in bone and gingival tissues. *Med Electron Microsc* 34:77–85.
41. Baldock PA, et al. (2007) Novel role of Y1 receptors in the coordinated regulation of bone and energy homeostasis. *J Biol Chem* 282:19092–19102.
42. Goto T, et al. (2007) Substance P stimulates late-stage rat osteoblastic bone formation through neurokinin-1 receptors. *Neuropeptides* 41:25–31.
43. Lundberg P, et al. (2007) Greater bone formation of Y2 knockout mice is associated with increased osteoprogenitor numbers and altered Y1 receptor expression. *J Biol Chem* 282:19082–19091.
44. Long H, Ahmed M, Ackermann P, Stark A, Li J (2010) Neuropeptide Y innervation during fracture healing and remodeling. A study of angulated tibial fractures in the rat. *Acta Orthop* 81:639–646.
45. Sample SJ, et al. (2014) Role of calcitonin gene-related peptide in functional adaptation of the skeleton. *PLoS One* 9:e113959.
46. Offley SC, et al. (2005) Capsaicin-sensitive sensory neurons contribute to the maintenance of trabecular bone integrity. *J Bone Miner Res* 20:257–267.
47. Heffner MA, Anderson MJ, Yeh GC, Genetos DC, Christiansen BA (2014) Altered bone development in a mouse model of peripheral sensory nerve inactivation. *J Musculoskelet Neuronal Interact* 14:1–9.

48. Rosemberg S, Marie SK, Kliemann S (1994) Congenital insensitivity to pain with anhidrosis (hereditary sensory and autonomic neuropathy type IV). *Pediatr Neurol* 11:50–56.
49. Toscano E, et al. (2000) Multisystem involvement in congenital insensitivity to pain with anhidrosis (CIPA), a nerve growth factor receptor(Trk A)-related disorder. *Neuropediatrics* 31:39–41.
50. Indo Y, et al. (2001) Congenital insensitivity to pain with anhidrosis (CIPA): Novel mutations of the TRKA (NTRK1) gene, a putative uniparental disomy, and a linkage of the mutant TRKA and PKLR genes in a family with CIPA and pyruvate kinase deficiency. *Hum Mutat* 18:308–318.
51. Bonkowsky JL, Johnson J, Carey JC, Smith AG, Swoboda KJ (2003) An infant with primary tooth loss and palmar hyperkeratosis: A novel mutation in the NTRK1 gene causing congenital insensitivity to pain with anhidrosis. *Pediatrics* 112:e237–e241.
52. Lane NE, et al. (2010) Tanezumab for the treatment of pain from osteoarthritis of the knee. *N Engl J Med* 363:1521–1531.
53. Hochberg MC (2015) Serious joint-related adverse events in randomized controlled trials of anti-nerve growth factor monoclonal antibodies. *Osteoarthritis Cartilage* 23: S18–S21.
54. Kawaja MD, et al. (2011) Nerve growth factor promoter activity revealed in mice expressing enhanced green fluorescent protein. *J Comp Neurol* 519:2522–2545.
55. Brault V, et al. (2001) Inactivation of the beta-catenin gene by Wnt1-Cre-mediated deletion results in dramatic brain malformation and failure of craniofacial development. *Development* 128:1253–1264.
56. Lee KCL, Maxwell A, Lanyon LE (2002) Validation of a technique for studying functional adaptation of the mouse ulna in response to mechanical loading. *Bone* 31: 407–412.
57. Tomlinson RE, Silva MJ (2015) HIF-1α regulates bone formation after osteogenic mechanical loading. *Bone* 73:98–104.
58. Dempster DW, et al. (2013) Standardized nomenclature, symbols, and units for bone histomorphometry: A 2012 update of the report of the ASBMR Histomorphometry Nomenclature Committee. *J Bone Miner Res* 28:2–17.
59. Hanefeld U, Rees CW, White AJP, Williams DJ (1996) One-pot synthesis of tetrasubstituted pyrazoles—proof of regiochemistry. *J Chem Soc, Perkin Trans 1* (13): 1545–1552.
60. Zerrate MC, et al. (2007) Neuroinflammation and behavioral abnormalities after neonatal terbutaline treatment in rats: Implications for autism. *J Pharmacol Exp Ther* 322:16–22.
61. Hargreaves K, Dubner R, Brown F, Flores C, Joris J (1988) A new and sensitive method for measuring thermal nociception in cutaneous hyperalgesia. *Pain* 32:77–88.
62. Mao J, et al. (1993) Intrathecal treatment with dextrorphan or ketamine potently reduces pain-related behaviors in a rat model of peripheral mononeuropathy. *Brain Res* 605:164–168.
63. Karl T, Pabst R, von Hörsten S (2003) Behavioral phenotyping of mice in pharmacological and toxicological research. *Exp Toxicol Pathol* 55:69–83.
64. Schindelin J, et al. (2012) Fiji: An open-source platform for biological-image analysis. *Nat Methods* 9:676–682.
65. Fulzele K, et al. (2010) Insulin receptor signaling in osteoblasts regulates postnatal bone acquisition and body composition. *Cell* 142:309–319.
66. Ke MT, Fujimoto S, Imai T (2013) SeeDB: A simple and morphology-preserving optical clearing agent for neuronal circuit reconstruction. *Nat Neurosci* 16:1154–1161.